Investigating human audio-visual object perception with a combination of hypothesis-generating and hypothesis-testing fMRI analysis tools

Marcus J. Naumer[1, 2, #, *], Jasper van den Bosch[1, #], Michael Wibral[3, #], Axel Kohler[4], Wolf Singer[5], Jochen Kaiser[1], Vincent van de Ven[2], Lars Muckli[6, 7]

[1] Institute of Medical Psychology, Goethe-University, Frankfurt am Main, Germany, [2] Faculty of Psychology and Neuroscience, Maastricht University, Maastricht, The Netherlands, [3] Brain Imaging Center, Goethe-University, Frankfurt am Main, Germany, [4] Department of Psychiatric Neurophysiology, University Hospital of Psychiatry, Bern, Switzerland, [5] Max Planck Institute for Brain Research, Frankfurt am Main, Germany, [6] Centre for Cognitive Neuroimaging (CCNi), Institute of Neuroscience and Psychology, University of Glasgow, Glasgow, U.K., [7] School of Psychology, University of Glasgow, Glasgow, U.K.

Electronic Supplementary Material

Supplementary Methods

On the number of components

The choice of number of components is a complicated issue in ICA analyses. Several quantitative solutions have been suggested in the literature, but as Calhoun et al. (2009) state in their review, the number of components remains a free parameter in spatial ICA of fMRI data. One complication of the quantitative solutions for the *optimal* number of components is that they depend on the kind of algorithm used and how functional data are prepared (cf., Calhoun et al. 2001; Beckmann and Smith 2005; Cordes and Nandy 2005). Moreover, all currently existing algorithms base their estimate on PCA decompositions (i.e., pre-whitened data), whereas ICA components are ultimately estimated using an objective

function for statistical independence. Thus, it is very likely that the algorithms may miss-specify the optimal dimensionality for ICA. Further, the analytical penalty for estimating too many components (over-estimation) is relatively limited and can be controlled by examining the correlations between the component time courses: If over-estimation results in splitting of a source into multiple components, the component time courses should be highly correlated. Conversely, with under-estimation, information is simply discarded from the analysis and cannot be retrieved. Finally, several authors (e.g., McKeown et al. 1998; Formisano et al. 2004; Abou-Elseoud et al. 2010) provide intuitive examples of cases in which full dimensionality (i.e., number of components equals number of measured volumes) revealed spatiotemporal dynamics that were not found with lower dimensionalities. Therefore, the existing algorithms by no means provide definitive estimations of ICA dimensionality. Thus, rather than true estimates of dimensionality, we regard these methods as quantitative heuristics that are at par with other, less complicated methods (e.g., Greicius et al. 2004; van de Ven et al. 2008; Abou-Elseoud et al. 2010).

An alternative heuristic to the number of components problem is to evaluate the reliability of decompositions of a particular dimensionality across multiple subjects. Our sogICA framework allows for such comparisons (e.g., van de Ven et al. 2008). We decomposed the functional time series of the participants of experiment 1 using 30, 35 and 40 components, and compared the degree of within-cluster spatial similarity (i.e., average spatial correlation between cluster members) of clusters of similar functional networks. Similarity measures did not differ ($P > 0.1$). However, we did find that for the 40-component decomposition some of the unisensory networks were split into multiple components in several participants, suggesting that this order of dimension was prone to over-fitting. Therefore, we chose to analyse our data using sICA of 35 components.

Decomposition and Clustering

Each individual set of volume time series was decomposed using sICA (McKeown et al. 1998; Calhoun et al. 2001; van de Ven et al. 2004) into 35 spatially independent components

and associated activation profiles. SICA was performed with FastICA (Hyvärinen 1999), using the deflation mode, which estimates each of the independent components successively. Before independent component estimation, the initial dimensions of the data were reduced to 35 using principal component analysis. After decomposition the spatial components and activation profiles were Z-scored (McKeown et al., 1998). Spatial components of all individual datasets were then grouped using a two-level data-driven clustering approach (van de Ven et al. 2009), using hierarchical clustering in which spatial correlations between component pairs were used as similarity measure (Esposito et al., 2005). On the first level, spatial components were clustered across the two experimental runs within each participant (within-subject clustering). Each experimental run of a participant contributed maximally one component to a cluster, yielding 35 clusters of 2 spatial components for each participant. Within each cluster the spatial components and associated activation profiles were averaged, and the mean cluster maps of each participant served as input to the second level (between-subject) clustering. Here, each participant contributed maximally one mean map to a second-level cluster, yielding 35 clusters of 10 first-level maps each. The resulting second-level (between-subject) clusters were ranked according to ascending intra-cluster distances, which is a measure of spatial similarity of cluster members (i.e., the cluster with best-matching components is ranked highest). For each between-subject cluster, a group map of the connectivity modes was generated by calculating a one-sample t-test statistic for the z-values at each voxel against a mean value of 0 (Esposito et al. 2005; van de Ven et al. 2008). The group t-maps were thresholded using the false discovery rate (FDR, Genovese et al. 2002; $q = 0.05$) to correct for multiple comparisons.

Selection of unisensory and AV clusters

The 35 cluster spatial maps were correlated with spatial templates of bilateral auditory cortex, primary and extrastriate visual cortex and left and right parietal cortex. Templates were derived from independent studies in which the functional time series were decomposed

using sICA (van de Ven et al. 2004; 2009). The cluster time courses were correlated with the ideal response profiles of unimodal and AV stimulus conditions of the first experiment. The ideal response profile was obtained by convolving the experimental design matrix with a hemodynamic response function. Clusters were selected according to their maximum spatial and temporal correlations. **Fig. S1** shows the spatial (r_{space}) and temporal (r_{time}) correlations for the three selected clusters. Note that the time course of the AV cluster correlated strongly with the unisensory and the AV response profile. However, the AV cluster's spatial map correlated only with left and right parietal cortex.

Supplementary Results

IC clustering

The group clustering results of the seven highest ranking IC clusters are shown in **Fig. S2**. The dispersion plot shows the intra- and intercluster distances (or dissimilarities) of the first seven clusters projected onto a 2-dimensional space using multidimensional scaling. This visualization procedure retained the relative distances between cluster members within and between clusters (Himberg et al. 2004; Esposito et al. 2005; van de Ven et al. 2008). The plot shows that sogICA generated spatially highly consistent clusters, with no cluster members of a cluster overlapping with the distribution of other clusters. We also calculated overlap maps to inspect the spatial distribution of the proportion of supra-threshold voxel values across participants. The overlap maps revealed a strong similarity and spatial selectivity between individual maps, which conforms to the results of the dispersion plot (right-hand panels of **Fig. S2**).

GLM analysis using cluster-size threshold for multiple comparison correction

In this procedure, the statistically uncorrected whole-brain GLM map of Experiment 1 (max-criterion; $P < 0.01$) was subjected to cluster–size statistical detection threshold estimation (Forman et al. 1995; Goebel et al. 2006), which simulated random activation maps based on the intrinsic smoothness of the source statistical map. This procedure was repeated 1000

times (Monte Carlo simulations). Each random simulation was then thresholded at the initial voxel threshold, and surviving voxel clusters were tabulated. Finally, the tabulated voxel cluster sizes were thresholded at a false-positive rate of 0.05. The minimum cluster size was used to correct the initial statistical map for multiple comparisons at the voxel cluster-level (1000 iterations). We revealed three regions (as shown in **Fig. S3)** which were located in right PFC, right pSTS, and left LOC regions. The first two regions showed considerable overlap with corresponding ROIs defined using ICA. During experiment 2 only the left LOC, but none of the other GLM-based ROIs met the criterion for AV convergence (AV > max[A, V]; $p<0.05$; **Fig. S3**).

Supplementary Figures

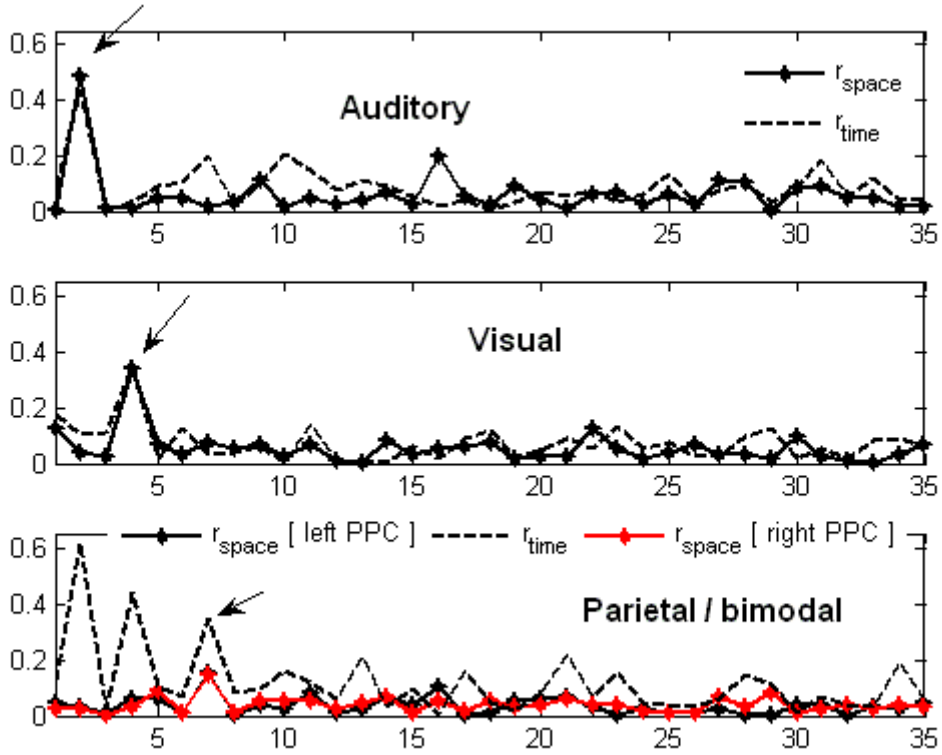

Figure S1. Spatial and temporal correlations for cluster selection.

Lines depict the absolute correlation coefficients between the cluster maps and spatial templates (solid; r_{space}) and between the cluster time courses and response profiles (broken; r_{time}). The bottom panel shows two sets of spatial correlations, between maps and a left (right) parietal template presented in black (red). For unisensory spatial templates the cluster with highest spatial correlation also correlated strongest with the unisensory response profile. For the parietal template only one cluster correlated highest (i.e., after the unisensory auditory and visual components) with the AV temporal profiles.

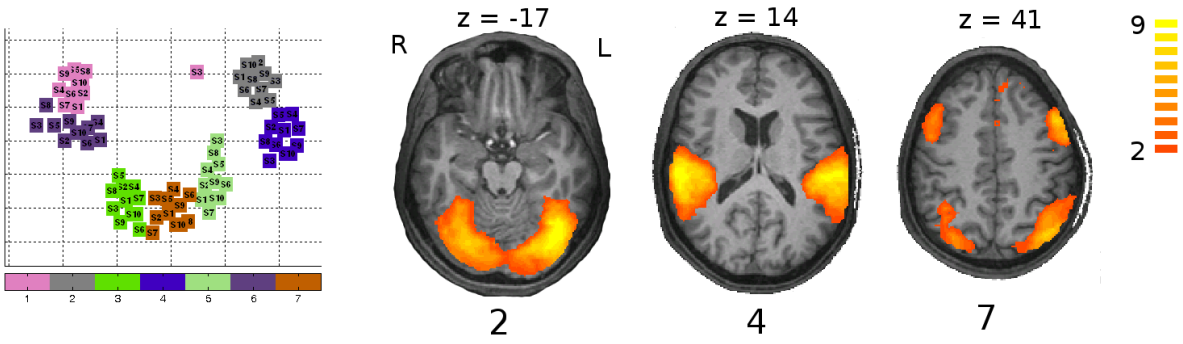

Figure S2. Independent component (IC) cluster distribution.

Dissimilarity measures are plotted for those seven IC clusters that showed the lowest mean intra-cluster distances (i.e., highest mean intra-cluster similarity). Left: 2-dimensional dispersion plot of intra-cluster dissimilarities; 2-D projection of the dissimilarities were estimated using multidimensional scaling. For the seven clusters, dispersion is dense, which suggests a high degree of similarity (i.e., very low dissimilarity). Clusters 2, 4 and 7 were selected as uni- and multisensory spatial modes (see text), cluster 1 reflected an EPI-related artifact (see **Fig. S4**). For details of plotting dissimilarity measures of sogICA, see previous publications (Esposito et al. 2005; van de Ven et al. 2008; Wibral 2007). Right: transversal view of the degree of overlap of the 10 constituent subject-level IC maps of each IC cluster of interest.

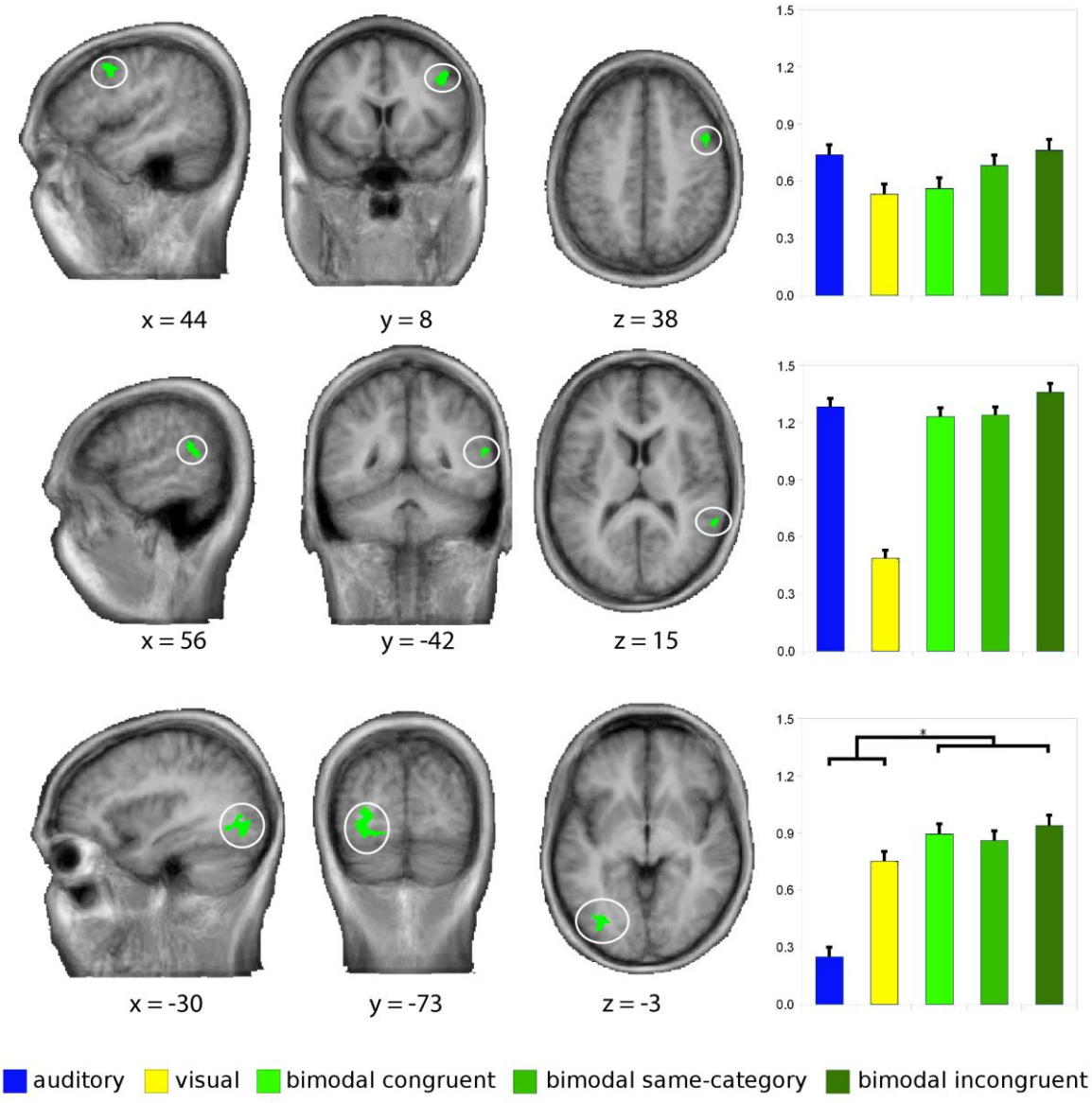

Figure S3. Comparison with GLM-based definition of AV integration regions.

AV convergence regions (AV > max[A, V]) were also defined on the basis of a conventional whole-brain GLM of experiment 1 (three regions surpassed the voxel cluster threshold). Graphs on the right show the respective functional activation profiles of these ROIs during experiment 2 by providing the GLM beta estimates for each experimental condition. The asterisk indicates the significance level of the max-contrast (*<0.05).

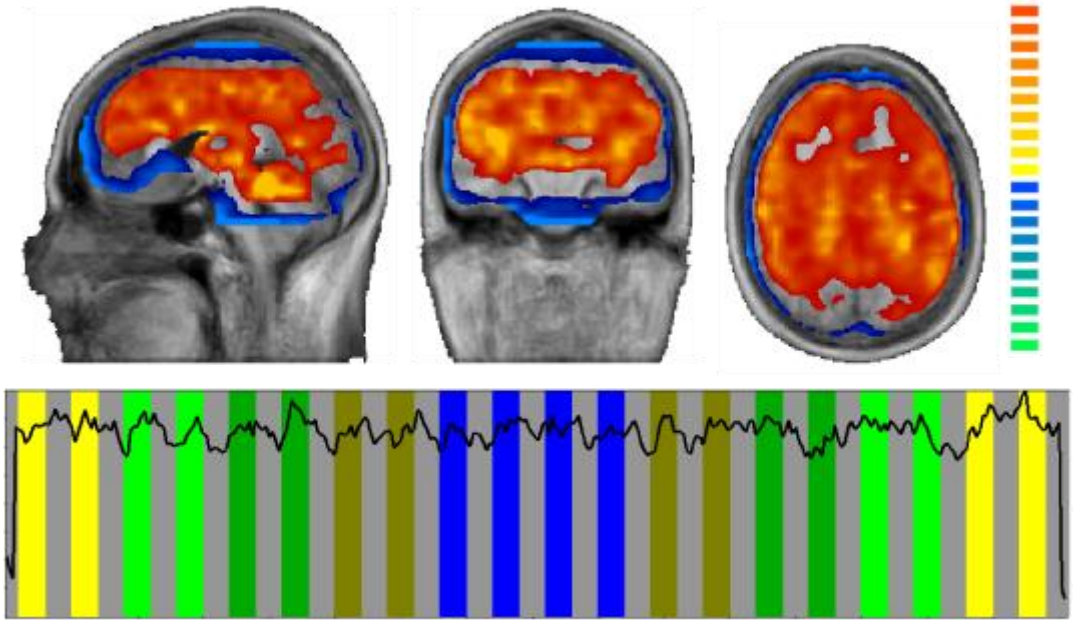

Figure S4. Artifactual independent component cluster.

We found between-subject clusters representing machine-related artefacts and clusters representing neurophysiologic activity of interest, similar to other ICA decompositions (McKeown et al. 1998; van de Ven et al. 2004; Esposito et al. 2005). The cluster with the highest intra-cluster similarity was associated with strong artifactual activation of a large contingent of voxels during all but the first and last volumes of their time course, most likely related to shim or B_0 field effects. Here we show the cluster map and time course for the artifactual IC cluster with the highest intra-cluster similarity. A similar data-driven result was reported previously (Esposito et al. 2005). For an overview of possible artifactual sources see Wibral 2007. For explanatory legend of experimental protocol, see main text.

Supplementary References

Abou-Elseoud A, Starck T, Remes J, Nikkinen J, Tervonen O, Kiviniemi V (2010) The effect of model order selection in group PICA. Hum. Brain Mapp. 31:1207-1216.

Beckmann CF, Smith SM (2005) Tensorial extensions of independent component analysis for multisubject fMRI analysis. Neuroimage 294-311.

Calhoun VD, Adali T, Pearlson GD, Pekar JJ (2001) Spatial and temporal independent component analysis of functional MRI data containing a pair of task-related waveforms. Hum. Brain Mapp. 13:43-53.

Calhoun VD, Liu J, Adali T (2009) A review of group ICA for fMRI data and ICA for joint inference of imaging, genetic, and ERP data. Neuroimage 45:S163-172.

Cordes D, Nandy RR (2005) Estimation of the intrinsic dimensionality of fMRI data. Neuroimage 29:145-154.

Esposito F, Scarabino T, Hyvarinen A, Himberg J, Formisano E, Comani S, Tedeschi G, Goebel R, Seifritz E, Di Salle F (2005) Independent component analysis of fMRI group studies by self-organizing clustering. Neuroimage 25:193-205.

Formisano E, Esposito F, Di Salle F, Goebel R (2004) Cortex-based independent component analysis. Magn. Res. Imag., 22:1493-1504.

Greicius MD, Srivastava G, Reiss AL, Menon V (2004) Default-mode network activity distinguishes Alzheimer's disease from healthy aging: evidence from functional MRI. Proc. Natl. Acad. Sci. U. S. A. 101:4637-4642.

Hyvärinen A (1999) Fast and robust fixed-point algorithms for independent component analysis. IEEE Trans. Neural Netw. 10:626-634.

McKeown MJ, Makeig S, Brown GG, Jung TP, Kindermann SS, Bell AJ, Sejnowski TJ (1998) Analysis of fMRI data by blind separation into independent spatial components. Hum. Brain Mapp. 6:160-188.

van de Ven V, Bledowski C, Prvulovic D, Goebel R, Formisano E, Di Salle F, Linden D E, Esposito F (2008) Visual target modulation of functional connectivity networks revealed by self-organizing group ICA. Hum. Brain Mapp. 29:1450-1461.

van de Ven V, Esposito F, Christoffels IK (2009) Neural network of speech monitoring overlaps with overt speech production and comprehension networks: A sequential spatial and temporal ICA study. Neuroimage 47:1982-1991.

van de Ven VG, Formisano E, Prvulovic D, Roeder CH, Linden DEJ (2004) Functional connectivity as revealed by spatial independent component analysis of fMRI measurements during rest. Hum. Brain Mapp. 22:165-178.

Wibral M (2007) The BOLD fMRI signal under anaesthesia and hyperoxia. Darmstadt (Germany): Electronic Publications Darmstadt (EPDA).